SketchyCoreSVD: SketchySVD from Random Subsampling of the Data Matrix

Chandrajit Bajaj, Yi Wang, Tianming Wang

Department of Computer Science, Oden Institute for Computational Engineering and Sciences,
University of Texas, Austin, Texas, USA.

August 1, 2019

Abstract

We present a method called SketchyCoreSVD to compute the near-optimal rank r SVD of a data matrix by building random sketches only from its subsampled columns and rows. We provide theoretical guarantees under incoherence assumptions, and validate the performance of our SketchyCoreSVD method on various large static and time-varying datasets.

1 Introduction

Data matrices in practice often have fast decaying spectrum. Finding low rank approximation to a data matrix is a fundamental task in numerous applications. Due to the massive size of data in modern applications, it may not be possible to store the full data matrix, causing problems for classic solvers.

It turns out that randomized sketches of the data matrix, built from dimension reduction maps, suffice for low-rank approximation. The first one-pass algorithm based on random sketches appear in [18]. Such ideas is further advocated in the survey article [8]. Ever since, quite a few algorithms [17, 4, 2, 13] based on random sketches have been developed. [1]

The most recent paper called SketchySVD [14] is shown to provide practical and consistent approximations compared to the predecessors. For a data matrix $\boldsymbol{A}$, SketchySVD finds the basis for the column/row space by QR decomposition of the left and right sketches while the first k singular values are well preserved in the core sketch. Theoretical guarantees have been derived for sketches built from Gaussian maps. The more practical dimension reduction maps such as Scrambled Subsampled Randomized Fourier Transform (SSRFT) [18] and sparse sign matrices [1, 9] are shown to exhibit similar performances in practice.

Building upon SketchySVD, we would like to claim that there is redundancy in the data matrix that can be further exploited when constructing sketches, thereby reducing the computation cost without sacrificing approximation accuracy. Such "redundancy" is characterized by incoherence[2], which is widely used in compressed sensing and matrix recovery. Several papers [11, 6, 3] also establish guarantees for Nyström method [16] based on the incoherence assumption. Overall, our contributions are the following:

---

[1]See Appendix A for a tabular summary description of prior sketch building algorithms.
[2]See Definition 1 in Section 2.2.

- Propose SketchyCoreSVD, a method to compute SketchySVD from subsampled columns and rows of the data matrix;

- Experiments verify that SketchyCoreSVD is able to reduce the computation cost of SketchySVD without sacrificing approximation accuracy;

- Theoretical guarantees based on incoherence assumption of the data matrix.

2 Algorithm

2.1 SketchyCoreSVD

Suppose the data matrix $A \in \mathbb{R}^{M \times N}$ is huge in size, and its spectrum is decaying fast enough for compression. Let r be a suitable choice of rank. The main goal is to find a near-optimal rank r approximation to A, via dimension reduction maps applied on subsampled columns and rows of A. Choose sketch sizes k and s such that $r \leq k \leq s \leq \min\{m, n, m', n'\}$, where m, n, m' and n' satisfy

$$\frac{m}{M} = \frac{n}{N} = p < 1, \quad \frac{m'}{M} = \frac{n'}{N} = q < 1, \quad \text{and} \quad p \leq q.$$

Inspired by SketchySVD [14], the steps of our method, termed SketchyCoreSVD, are the following.

1. Building sketches.

    - Uniformly sample (without replacement) m rows of A. Denote the indices of the sampled rows to be Δ. The map $\Gamma \in \mathbb{R}^{k \times m}$ is applied to $A^{(\Delta,:)}$ from the left,

    $$X = \Gamma A^{(\Delta,:)} \in \mathbb{R}^{k \times N};$$

    - Uniformly sample (without replacement) n columns of A. Denote the indices of the sampled columns to be Θ. The map $\Omega \in \mathbb{R}^{k \times n}$ is applied to $A^{(:,\Theta)}$ from the right,

    $$Y = A^{(:,\Theta)} \Omega^* \in \mathbb{R}^{M \times k};$$

    - Uniformly sample (without replacement) m' row indices and n' column indices, denoted by Δ' and Θ', respectively. Apply random matrix maps $\Phi \in \mathbb{R}^{s \times m'}$ and $\Psi \in \mathbb{R}^{s \times n'}$ to the intersection of $A^{(\Delta',\Theta')} \in \mathbb{R}^{m' \times n'}$, i.e.,

    $$Z = \Phi A^{(\Delta',\Theta')} \Psi^* \in \mathbb{R}^{s \times s}.$$

2. Computations.

    - We compute the QR decomposition of X^*,

    $$X^* = PR_1,$$

    where $P \in \mathbb{R}^{N \times k}$, and $R_1 \in \mathbb{R}^{k \times k}$;

    - We compute the QR decomposition of Y,

    $$Y = QR_2,$$

    where $Q \in \mathbb{R}^{M \times k}$, and $R_2 \in \mathbb{R}^{k \times k}$;

- We compute the core approximation,

$$\boldsymbol{C} = (\boldsymbol{\Phi Q}^{(\Delta',:)})^\dagger \cdot \boldsymbol{Z} \cdot ((\boldsymbol{\Psi P}^{(\Theta',:)})^\dagger)^* \in \mathbb{R}^{k \times k};$$

- Denote $\hat{\boldsymbol{A}} = \boldsymbol{QCP}^*$ as the initial approximation. The final near-optimal rank r approximation to $\boldsymbol{A}$, denoted by $[[\hat{\boldsymbol{A}}]]_r$, is computed by

$$\boldsymbol{Q}[[\boldsymbol{C}]]_r \boldsymbol{P}^*,$$

where $[[\boldsymbol{C}]]_r$ is the best rank r approximation to $\boldsymbol{C}$.

While the storage cost is the same, SketchyCoreSVD has reduced computational cost. The following table shows the flops count of the two methods for Gaussian maps. If the same k and s are used, Sketchy-CoreSVD has lower complexity. The cost is reduced mainly when constructing the sketches.

	SketchySVD	SketchyCoreSVD
$\boldsymbol{X}$	$O(kMN)$	$O(kpMN)$
$\boldsymbol{Y}$	$O(kMN)$	$O(kMN)$
$\boldsymbol{Z}$	$O(sMN + s^2 \min\{M, N\})$	$O(sq^2MN + s^2q \min\{M, N\})$
QR of $\boldsymbol{X}$	$O(k^2N)$	$O(k^2N)$
QR of $\boldsymbol{Y}$	$O(k^2M)$	$O(k^2M)$
$\boldsymbol{C}$	$O(k^2s + ks^2 + ks(M+N))$	$O(k^2s + ks^2 + ksq(M+N))$
$[[\boldsymbol{C}]]_r$	$O(k^3)$	$O(k^3)$
$[[\hat{\boldsymbol{A}}]]_r$	$O(kr(M+N) + r^2 \min\{M,N\} + rMN)$	$O(kr(M+N) + r^2 \min\{M,N\} + rMN)$

2.2 Theoretical Guarantees

Our proofs generally follow the outline of [14], though with substantial differences when dealing with subsamples of the data matrix. The fist step is to prove that $\boldsymbol{Q}$ and $\boldsymbol{P}$ capture the range and co-range of $\boldsymbol{A}$, which are expressed as

$$\boldsymbol{A} \approx \boldsymbol{QQ}^*\boldsymbol{A}, \quad \boldsymbol{A} \approx \boldsymbol{APP}^*.$$

These are proved in [8] for $\boldsymbol{Q}$ and $\boldsymbol{P}$ computed from the sketches of the full matrix. For our case, only a randomly selected subsets of the columns/rows are used. Thus we must impose certain conditions on the columns/rows of $\boldsymbol{A}$.

The intuition is that the columns/rows are "more or less the same". Such a matrix property can be characterized by incoherence. Suppose $\boldsymbol{A} \in \mathbb{R}^{M \times N}$ has an SVD of the following form

$$\boldsymbol{U\Sigma V}^* = \begin{bmatrix} \boldsymbol{U}_1 & \boldsymbol{U}_2 \end{bmatrix} \begin{bmatrix} \boldsymbol{\Sigma}_1 & \\ & \boldsymbol{\Sigma}_2 \end{bmatrix} \begin{bmatrix} \boldsymbol{V}_1 & \boldsymbol{V}_2 \end{bmatrix}^*,$$

where $[[\boldsymbol{A}]]_r = \boldsymbol{U}_1 \boldsymbol{\Sigma}_1 \boldsymbol{V}_1^*$ is the best rank r approximation of $\boldsymbol{A}$.

Definition 1. $[[\boldsymbol{A}]]_r \in \mathbb{R}^{M \times N}$ *is (μ, ν)-incoherent if*

$$\max_i \left\{ \|\boldsymbol{U}_1^{(i,:)}\|_2 \right\} \leq \sqrt{\frac{\mu r}{M}} \quad and \quad \max_j \left\{ \|\boldsymbol{V}_1^{(j,:)}\|_2 \right\} \leq \sqrt{\frac{\nu r}{N}}.$$

3

Based on the incoherence assumption, we provide the following error bound.

Theorem 1. *Suppose $A = U_1\Sigma_1V_1^* + U_2\Sigma_2V_2^*$, where $[[A]]_r = U_1\Sigma_1V_1^*$, the best rank r approximation of A, is (μ, ν)-incoherent. Then for our SketchyCoreSVD algorithm with $k \geq r + 4$, $m \geq 8\mu r \log r$ and $n \geq 8\nu r \log r$,*

$$\max\{\|A - QQ^*A\|_F, \|A - APP^*\|_F\} \leq (C_1(p,k,r) + 1) \cdot \|\Sigma_2\|_F + C_2(p,k,r) \cdot \|\Sigma_2\|_2$$

with probability at least $1 - \frac{4}{r^3} - \frac{4}{k^3}$, where

$$C_1(p,k,r) = \sqrt{\frac{6e^2}{p} \cdot \frac{k}{k - r + 1}} \cdot k^{\frac{3}{k-r+1}} \quad and \quad C_2(p,k,r) = \sqrt{\frac{36e^2}{p} \cdot \frac{\sqrt{k \log k}}{k - r + 1}} \cdot k^{\frac{3}{k-r+1}}.$$

Remark. *Note that $C_1(p,k,r)$ and $C_2(p,k,r)$ both decrease as p or k increases. Thus we are advised to use a not too small sampling ratio p, and a bigger sketch size k whenever possible.*

Let Q and P be the basis computed by SketchyCoreSVD for the columns and rows, respectively. There exist $\mu' \in [1, M]$ and $\nu' \in [1, N]$ such that

$$\max_i\left\{\|Q^{(i,:)}\|_2\right\} \leq \sqrt{\frac{\mu'k}{M}} \quad and \quad \max_j\left\{\|P^{(j,:)}\|_2\right\} \leq \sqrt{\frac{\nu'k}{N}}.$$

The existence of μ' and ν' can be easily shown.[3] We derive the following guarantee for the rank r approximation $[[\hat{A}]]_r$ computed by SketchyCoreSVD, provided that m' and n' are greater than some multiples of $\mu'k \log k$ and $\nu'k \log k$, respectively.

Theorem 2. *Condition on the success of Theorem 1, for our SketchyCoreSVD algorithm with $s \geq k + 4$, $m' \geq 8\mu'k \log k$, and $n' \geq 8\nu'k \log k$, the initial approximation $\hat{A}$ satisfies*

$$\|A - \hat{A}\|_F \leq C_3(p,q,s,k,r) \cdot \|\Sigma_2\|_F + C_4(p,q,s,k,r) \cdot \|\Sigma_2\|_2$$

with probability at least $1 - \frac{4}{k^3} - \frac{6}{s^3}$, where

$$C_3(p,q,s,k,r) = C_1(p,k,r)\cdot(\sqrt{3}C(q,s,k)+\sqrt{2}), \quad C_4(p,q,s,k,r) = C_2(p,k,r)\cdot(\sqrt{3}C(q,s,k)+\sqrt{2}),$$

$$C(q,s,k) = \frac{6e^2}{q} \cdot \frac{s^{1+6/(s-k+1)}}{(s-k+1)^2} \cdot \left(\sqrt{s} + \sqrt{6\log s}\right)^2.$$

Moreover, the final rank r approximation satisfies

$$\|A - [[\hat{A}]]_r\|_F \leq (2C_3(p,q,s,k,r) + 1) \cdot \|\Sigma_2\|_F + (2C_4(p,q,s,k,r)) \cdot \|\Sigma_2\|_2.$$

Remark. *Note that $C(q,s,k)$ decreases as q or s increases. Thus we are advised to use a not too small sampling ratio q, and a bigger sketch size s whenever possible.*

We admit the dependence on μ' and ν' is the deficiency of our current theoretical guarantees. Ideally, one should derive bounds for μ' and ν' based on μ and ν. One way to get around this is to slightly modify the algorithm: after building the left and right sketches, we calculate the QR factorizations, and sample m' row indices and n' column indices based on the actual incoherence parameters, estimated from the row norms, of Q and P, respectively.

Nevertheless, we observe that $\mu' = O(\mu)$, $\nu' = O(\nu)$ in practice.[4] In the experiments shown in Section 3, we simply choose $m' = m$ and $n' = n$, i.e., $q = p$.

---

[3]For example, consider μ'. Since $\max_i\{\|Q^{(i,:)}\|_2^2\} \leq k$, it follows that $\mu' \leq M$. If $\mu' < 1$, then $\|Q\|_F^2 < M \cdot \frac{k}{M} = k$, contradicting to the fact that $\|Q\|_F^2 = k$.

[4]See Table 6 for some empirical evidences.

3 Numerical Experiments

If full SVD can be computed, the guide to choose the rank is to find the "knee" in the scree plot. At rank r,

$$scree(r) = \frac{1}{\|\boldsymbol{A}\|_F^2} \sum_{i=r+1} \sigma_i^2(\boldsymbol{A}).$$

For a rank r approximation $[[\hat{\boldsymbol{A}}]]_r$ to $\boldsymbol{A}$, we measure its approximation error as

$$err = \frac{\|[[\hat{\boldsymbol{A}}]]_r - \boldsymbol{A}\|_F^2}{\|\boldsymbol{A}\|_F^2}.$$

We compare our SketchyCoreSVD method to SketchySVD [14], which suggests one to choose $s \geq 2k+1$ and $k = O(r)$. The dimension reduction maps used are Gaussian maps. For our SketchyCoreSVD, we choose the sampling ratio p such that $p \cdot \min\{M, N\} \geq s$, and $q = p$.

The experiments are executed from MATLAB R2018a on a 64-bit Linux machine with 8 Intel i7-7700 CPUs at 3.60 GHz and 32 GB of RAM. The reported errors are averaged over 20 trials. In the experiments, we first load the data into memory and then build the sketches. The computation time reported does not include computing the final approximation $[[\hat{\boldsymbol{A}}]]_r$ since in practice it is usually stored in the factorized form for subsequent tasks. The need to compute $[[\hat{\boldsymbol{A}}]]_r$ is only for the error metric. We also provide visual comparisons on the first few left singular vectors in each case.

3.1 Yale Face Dataset

The data is originally from the Yale Face Database B [5]. For this dataset, $\boldsymbol{A} \in \mathbb{R}^{2500 \times 640}$ since there are 640 face images of size 50×50. Based on the scree plot, we choose $r = 20$. The optimal err is 0.033.
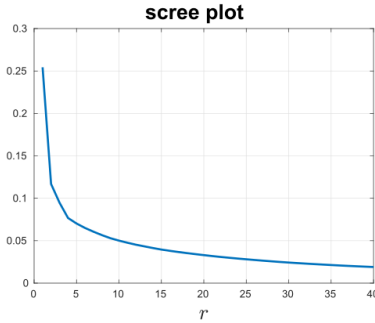
Figure 1: Scree plot for Yale Face dataset.

	SketchySVD	SketchyCoreSVD		
p	-	0.3	0.35	0.4
err	0.066	0.0765	0.0737	0.0717
time (sec)	0.0239	0.0134	0.0146	0.0166

Table 1: Performance comparisons for Yale Face dataset.

5

We choose $k = 4r + 1 = 81$ and $s = 2k + 1 = 163$ for both methods. In Table 1, we see that the error of SketchySVD is about twice the optimal error. Our SketchyCoreSVD can achieve about the same error bound with less time . As the sampling ratio p increases from 30% to 40%, the err decreases while computation time only gradually increases. In the visual comparison Figure 2, we show that the singular vector(s) can be estimated accurately, and with sampling ratio $p = 40\%$ for SketchyCoreSVD.

Figure 2: Visual comparison for the first left singular vector computed on the Yale Face dataset. Ground truth (left column), SketchySVD (middle column), SketchyCoreSVD (right column, $p = 0.4$). The peak signal to noise ratio (PSNR) is 44.0320 for SketchySVD, and 44.2639 for SketchyCoreSVD.

3.2 Cardiac Magnetic Resonance Imaging

We have a collection of time-varying, 2D slice stacks of cardiac magnetic resonance images (Cardiac MRI). We select a 2D MR spatial snapshot and consider a time-sequence of this in the form of a data matrix $A \in \mathbb{R}^{45056 \times 160}$ (i.e., 160 time snapshots 2D images, each of of size 256×176). Based on the scree plot, we choose $r = 5$. The optimal err is 0.0011.
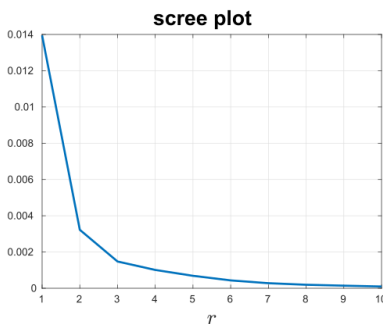
Figure 3: Scree plot for Cardiac MRI dataset.

We choose $k = 4r + 1 = 21$ and $s = 2k + 1 = 43$ for both methods. In Table 2, we see that the error of SketchySVD is less than twice the optimal error. Our SketchyCoreSVD can achieve the same error bound in less time. As sampling ratio p increases from 30% to 40%, err decreases while computation time gradually increases. In the visual comparison Figure 4, we show that the singular vector(s) can be estimated accurately, and with sampling ratio $p = 40\%$ for SketchyCoreSVD.

6

	SketchySVD	SketchyCoreSVD		
p	-	0.3	0.35	0.4
err	0.0019	0.0021	0.0021	0.0019
time (sec)	0.0567	0.0316	0.038	0.0396

Table 2: Performance comparisons for Cardiac MRI dataset.
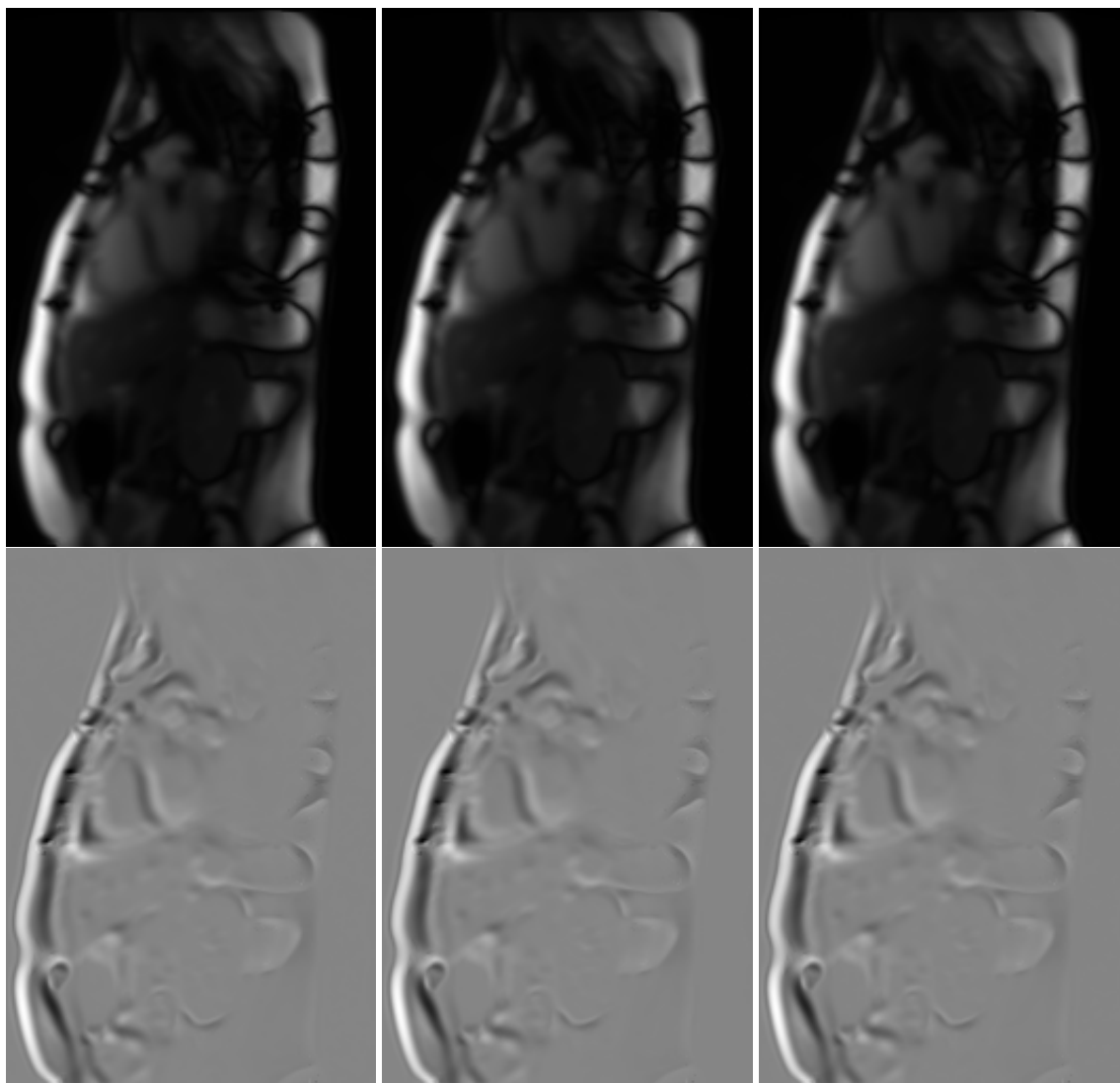
Figure 4: Visual comparison for the first two left singular vectors computed on the Cardiac MRI dataset. Ground truth (left column), SketchySVD (middle column), SketchyCoreSVD (right column, $p = 0.4$). The PSNR values are $\{68.5232, 59.1094\}$ for SketchySVD, and $\{69.5770, 58.3338\}$ for SketchyCoreSVD.

3.3 The BR1003 Breast Cancer Dataset

This breast cancer data matrix we use is extracted from a collection of Fourier-transform infrared spectroscopy (FTIR) spectral signatures of breast tissues [7]. The matrix $A \in \mathbb{R}^{1506 \times 783090}$ is created from 789030 spectral signatures of length 1506. Based on the scree plot, we choose $r = 6$. The optimal err is 0.002.
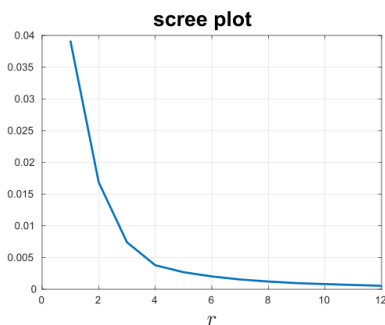
Figure 5: Scree plot for BR1003 dataset.

	SketchySVD	SketchyCoreSVD		
p	-	0.04	0.06	0.08
err	0.0025	0.0031	0.0029	0.0027
time (sec)	3.2049	0.816	1.1643	1.3614

Table 3: Performance comparisons for BR1003 dataset.
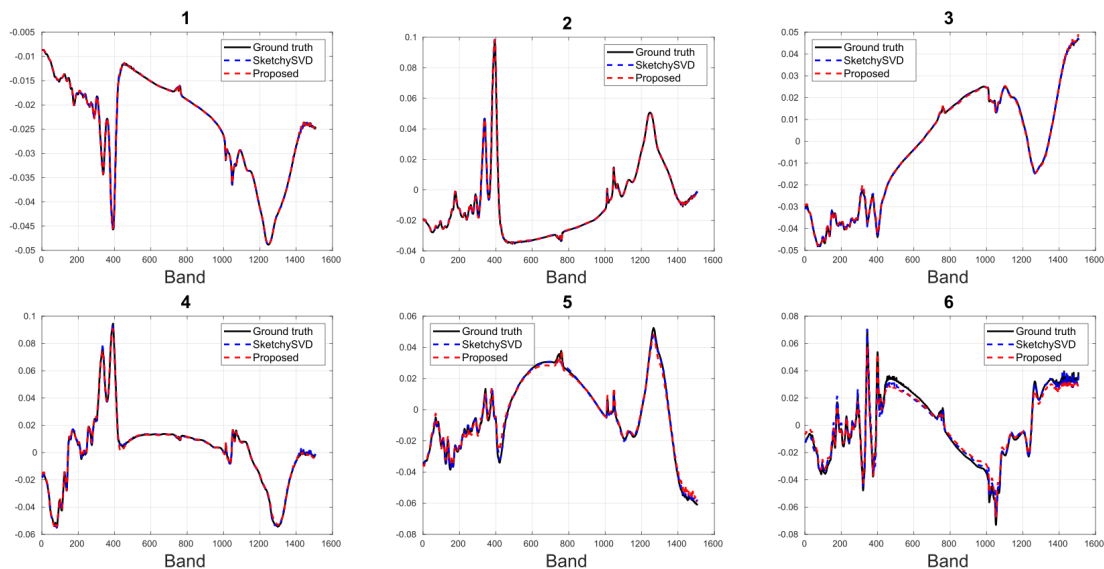
Figure 6: Visual comparison for the first six left singular vectors computed on the BR1003 dataset, where $p = 0.08$ for our SketchyCoreSVD method.

	1	2	3	4	5	6
SketchySVD	56.6010	41.9409	37.9187	32.6139	25.3890	18.6244
SketchyCoreSVD	54.2577	39.0797	34.9353	31.8365	23.0102	15.6122

Table 4: Comparison of signal to noise (SNR) ratios for the first six left singular vectors computed on the BR1003 dataset, where $p = 0.08$ for our SketchyCoreSVD method.

We choose $k = 4r + 1 = 25$ and $s = 2k + 1 = 51$ for both methods. In Table 3, we see that the error of SketchySVD is about the same as the optimal error. SketchyCoreSVD can achieve about the same error bound in less than half of the time. As the sampling ratio p increases from 4% to 8%, the err decreases while the computation time only gradually increases. In the visual comparison Figure 6, we show that the singular vector(s) can be estimated accurately, and with sampling ratio $p = 8\%$ for SketchyCoreSVD.

3.4 Video Dataset

This dataset is a color video of size $1080 \times 1920 \times 3 \times 2498$. It was originally used by [10] to test tensor approximations. We converted the video into to grayscale, reduced the spatial size by a factor of 2, and discarded the first 100 and last 198 frames due to camera blur. The resulting data matrix $A \in \mathbb{R}^{518400 \times 2200}$. Based on the scree plot, we choose $r = 25$. The optimal err is 0.0066.
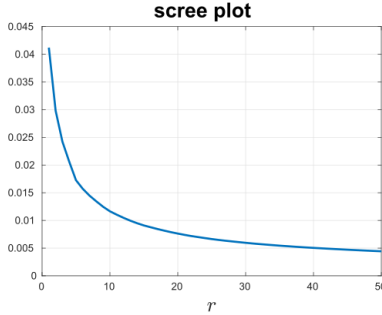
Figure 7: Scree plot for Video dataset.

	SketchySVD	SketchyCoreSVD		
p	-	0.1	0.15	0.2
err	0.0148	0.0213	0.0177	0.0165
time (sec)	8.0062	2.3224	2.6266	3.5619

Table 5: Performance comparisons for Video dataset.

We choose $k = 4r + 1 = 101$ and $s = 2k + 1 = 203$ for both methods. In Table 4, we see that the error of SketchySVD is about twice the optimal error. SketchyCoreSVD can achieve about the same error bound in less than half of the time. As the sampling ratio p is increased from 10% to 20%, the err decreases while the computation time only gradually increases. In the visual comparison Figure 8, we show that the singular vector(s) can be estimated accurately, and with sampling ratio $p = 20\%$ for SketchyCoreSVD.

9

Figure 8: Visual comparison for the first two left singular vectors computed on the Video dataset. Ground truth (left column), SketchySVD (middle column), SketchyCoreSVD (right column, $p = 0.2$). The PSNR values are $\{55.5701, 50.2379\}$ for SketchySVD, and $\{55.8322, 49.2919\}$ for SketchyCoreSVD.

References

[1] Dimitris Achlioptas. Database-friendly random projections: Johnson-Lindenstrauss with binary coins. *Journal of computer and System Sciences*, 66(4):671–687, 2003.

[2] Christos Boutsidis, David P Woodruff, and Peilin Zhong. Optimal principal component analysis in distributed and streaming models. In *Proceedings of the forty-eighth annual ACM symposium on Theory of Computing*, pages 236–249. ACM, 2016.

[3] Jiawei Chiu and Laurent Demanet. Sublinear randomized algorithms for skeleton decompositions. *SIAM Journal on Matrix Analysis and Applications*, 34(3):1361–1383, 2013.

[4] Michael B Cohen, Sam Elder, Cameron Musco, Christopher Musco, and Madalina Persu. Dimensionality reduction for k-means clustering and low rank approximation. In *Proceedings of the forty-seventh annual ACM symposium on Theory of computing*, pages 163–172. ACM, 2015.

[5] A.S. Georghiades, P.N. Belhumeur, and D.J. Kriegman. From few to many: illumination cone models for face recognition under variable lighting and pose. *IEEE Transactions on Pattern Analysis and Machine Intelligence*, 23(6):643–660, June 2001.

[6] Alex Gittens. The spectral norm error of the naive nystrom extension. *arXiv preprint arXiv:1110.5305*, 2011.

[7] Soumyajit Gupta, Shachi Mittal, Andre Kajdacsy-Balla, Rohit Bhargava, and Chandrajit Bajaj. A fully automated, faster noise rejection approach to increasing the analytical capability of chemical imaging for digital histopathology. *PLOS ONE*, 14(4):1–15, 04 2019.

[8] Nathan Halko, Per-Gunnar Martinsson, and Joel A Tropp. Finding structure with randomness: Probabilistic algorithms for constructing approximate matrix decompositions. *SIAM review*, 53(2):217–288, 2011.

[9] Ping Li, Trevor J Hastie, and Kenneth W Church. Very sparse random projections. In *Proceedings of the 12th ACM SIGKDD international conference on Knowledge discovery and data mining*, pages 287–296. ACM, 2006.

[10] Osman Asif Malik and Stephen Becker. Low-rank Tucker decomposition of large tensors using TensorSketch. In *Advances in Neural Information Processing Systems*, pages 10096–10106, 2018.

[11] Ameet Talwalkar and Afshin Rostamizadeh. Matrix coherence and the Nystrom method. *arXiv preprint arXiv:1408.2044*, 2014.

[12] Joel A Tropp. Improved analysis of the subsampled randomized Hadamard transform. *Advances in Adaptive Data Analysis*, 3(01n02):115–126, 2011.

[13] Joel A Tropp, Alp Yurtsever, Madeleine Udell, and Volkan Cevher. Practical sketching algorithms for low-rank matrix approximation. *SIAM Journal on Matrix Analysis and Applications*, 38(4):1454–1485, 2017.

[14] Joel A Tropp, Alp Yurtsever, Madeleine Udell, and Volkan Cevher. Streaming low-rank matrix approximation with an application to scientific simulation. *arXiv preprint arXiv:1902.08651*, 2019.

[15] Jalaj Upadhyay. The price of privacy for low-rank factorization. In *Advances in Neural Information Processing Systems*, pages 4176–4187, 2018.

[16] Christopher Williams and Matthias Seeger. Using the Nyström method to speed up kernel machines. In *Advances in neural information processing systems*, pages 682–688, 2001.

[17] David P Woodruff et al. Sketching as a tool for numerical linear algebra. *Foundations and Trends® in Theoretical Computer Science*, 10(1–2):1–157, 2014.

[18] Franco Woolfe, Edo Liberty, Vladimir Rokhlin, and Mark Tygert. A fast randomized algorithm for the approximation of matrices. *Applied and Computational Harmonic Analysis*, 25(3):335–366, 2008.

A Algorithms Based on Sketches

We provide a brief comparison of prior algorithms based on sketches.

---

[8] builds sketches
$$X = \Gamma A \quad \text{and} \quad Y = A\Omega^*.$$
Compute $(P, \sim, \sim) = \text{svds}(X^*, r)$, $(Q, \sim, \sim) = \text{svds}(Y, r)$; $C_1 = Q^*Y\left((\Omega P)^\dagger\right)^*$, $C_2 = (\Gamma Q)^\dagger X P$; $(U, \Sigma, V) = \text{svd}((C_1 + C_2)/2)$;
$$\hat{A} = (QU)\Sigma(PV)^*.$$

---

[17] builds sketches
$$X = \Gamma A \quad \text{and} \quad Y = A\Omega^*.$$
Compute $Y = QR$; $\Gamma Q = UT$;
$$\hat{A} = QT^\dagger[[U^*Y]]_r.$$

<div style="border:1px solid">

[4] builds sketches
$$X = \Gamma A \quad \text{and} \quad Y = A\Omega^*.$$

Compute $(V, \sim, \sim) = \mathrm{svds}(Y, r)$; $\Gamma Q = UT$;

$$\hat{A} = VT^\dagger[[U^* Y]]_r.$$

</div>

<div style="border:1px solid">

[2] with simplification suggested by **[15]**. Build sketches
$$X = \Gamma A, \quad Y = A\Omega^*, \quad \text{and} \quad Z = \Phi A \Psi^*.$$

Compute $X^* = PR_1, Y = QR_2$; $\Phi Q = U_1 \Sigma_1 V_1^*$, $\Psi P = U_2 \Sigma_2 V_2^*$;

$$\hat{A} = QV_1\Sigma_1^\dagger[[U_1^* Z U_2]]_r \Sigma_2^\dagger V_2^* P^*.$$

</div>

<div style="border:1px solid">

[13] builds sketches
$$X = \Gamma A \quad \text{and} \quad Y = A\Omega^*.$$

Compute $Y = QR$;

$$\hat{A} = Q[[(\Gamma Q)^\dagger X]]_r.$$

</div>

B Proof of Theorem 1

The following proofs are for the approximation of the column space of A, i.e., $\|A - QQ^* A\|_F$. Similar argument holds for $\|A - APP^*\|_F$.

We first state a few auxiliary lemmas to facilitate the presentation of the main proof of Theorem 1. Lemma 1, adapted from [12, Lemma 3.4], is essential for our proofs since it provides a lower bound on the singular values of a submatrix from randomly sampled rows of an "incoherent" orthonormal matrix.

Lemma 1. *Suppose* $\max_j\{\|V_1^{(j,:)}\|_2\} \le \sqrt{\frac{\mu r}{N}}$. *For* $\alpha > 0$, *select the sample size*

$$n \ge 8\mu r \log r.$$

Draw a random subset Θ *from* $\{1, \cdots, N\}$ *by sampling* n *coordinates without replacement. Then with probability at least* $1 - \frac{2}{r^3}$,

$$\sqrt{\frac{n}{6N}} \le \sigma_r(V_1^{(\Theta,:)}) \quad and \quad \sigma_1(V_1^{(\Theta,:)}) \le \sqrt{\frac{13n}{6N}}.$$

If we further apply Gaussian maps to the subsampled rows, Lemma 2 ensures that the full rankness is preserved almost surely.

Lemma 2. *Suppose* $V_1^{(\Theta,:)} \in \mathbb{R}^{n \times r}$ *is of full column rank, and* $\Omega \in \mathbb{R}^{k \times n}$ *is standard normal Gaussian. Then* $\Omega V_1^{(\Theta,:)} \in \mathbb{R}^{k \times r}$ *is of full column rank almost surely.*

Proof. We prove for $\Omega V_1^{(\Theta,:)}$. From Lemma 1, we know that $V_1^{(\Theta,:)}$ is of full column rank. Denote its truncated SVD by $W_1 \Lambda W_2^*$, where $W_1 \in \mathbb{R}^{n \times r}$, $\Lambda \in \mathbb{R}^{r \times r}$, and $W_2 \in \mathbb{R}^{r \times r}$. Since W_1 is orthonormal, $\Omega W_1 \in \mathbb{R}^{k \times r}$ is standard Gaussian. Thus with probability one, ΩW_1 is of full column rank. Consequently, $\Omega V_1^{(\Theta,:)} = (\Omega W_1)\Lambda W_2^*$ is also of full column rank. $\square$

From Lemma 2, we know that $(\boldsymbol{V}_1^*)^{(:,\Theta)}\boldsymbol{\Omega}^* \in \mathbb{R}^{r \times k}$ is of full row rank. Define $\boldsymbol{\Omega}_1 = (\boldsymbol{V}_1^*)^{(:,\Theta)}\boldsymbol{\Omega}^*$, and $\boldsymbol{\Omega}_2 = (\boldsymbol{V}_2^*)^{(:,\Theta)}\boldsymbol{\Omega}^*$. Lemma 3 below provides a deterministic bound of $\|\boldsymbol{A} - \boldsymbol{Q}\boldsymbol{Q}^*\boldsymbol{A}\|_F^2$. It can be proved similarly as [8, Theorem 9.1]. For completeness, we include its proof in Section B.1.

Lemma 3. *Assuming that $\boldsymbol{\Omega}_1 \in \mathbb{R}^{r \times k}$ has full row rank, and $\boldsymbol{Q} \in \mathbb{R}^{M \times k}$ is the orthonormal columns from the QR decomposition of $\boldsymbol{A}^{(:,\Theta)}\boldsymbol{\Omega}$. Then*

$$\|\boldsymbol{A} - \boldsymbol{Q}\boldsymbol{Q}^*\boldsymbol{A}\|_F^2 \leq \|\boldsymbol{\Sigma}_2\|_F^2 + \|\boldsymbol{\Sigma}_2\boldsymbol{\Omega}_2\boldsymbol{\Omega}_1^\dagger\|_F^2, \tag{1}$$

where $\boldsymbol{\Sigma}_2$ is the diagonal matrix containing the $(r+1)$ to $\min\{M, N\}$ singular values of $\boldsymbol{A}$.

For the bound in (1), $\boldsymbol{\Omega}_2$ and $\boldsymbol{\Omega}_1$ are not independent in our case, contrary to what [14] deals with. Our strategy is to separately bound $\boldsymbol{\Sigma}_2\boldsymbol{\Omega}_2$ and $\boldsymbol{\Omega}_1^\dagger$. For $\boldsymbol{\Omega}_1^\dagger$, we need to deal with the operator norm of the pseudo-inverse of random Gaussian at some point. Lemma 4, adapted from [8, Proposition 10.3], provides such a bound.

Lemma 4. *For $\boldsymbol{G} \in \mathbb{R}^{k \times r}$ ($k \geq r + 4$) being standard normal Gaussian,*

$$\mathbb{P}\left\{\|\boldsymbol{G}^\dagger\|_2 \geq \frac{e\sqrt{k}}{k - r + 1} \cdot t\right\} \leq t^{-(k-r+1)}, \quad \forall t \geq 1.$$

Taking $t = k^{\frac{3}{k-r+1}}$, then

$$\|\boldsymbol{G}^\dagger\|_2 \leq \frac{e\sqrt{k}}{k - r + 1} \cdot k^{\frac{3}{k-r+1}}$$

with probability at least $1 - \frac{1}{k^3}$.

We bound $\|\boldsymbol{\Sigma}_2\boldsymbol{\Omega}_2\|_F$ with the help of Lemma 5 and Lemma 6.

Lemma 5. *([8, Proposition 10.1]) Fix matrices $\boldsymbol{S}$, $\boldsymbol{T}$, and draw a standard Gaussian matrix $\boldsymbol{G}$. Then*

$$\mathbb{E}(\|\boldsymbol{S}\boldsymbol{G}\boldsymbol{T}\|_F^2) = \|\boldsymbol{S}\|_F^2\|\boldsymbol{T}\|_F^2.$$

Lemma 6. *([8, Proposition 10.3]) Suppose h is a Lipschitz function on matrices:*

$$|h(\boldsymbol{X}) - h(\boldsymbol{Y})| \leq L\|\boldsymbol{X} - \boldsymbol{Y}\|_F, \quad \forall \boldsymbol{X}, \boldsymbol{Y}.$$

Draw a standard Gaussian matrix $\boldsymbol{G}$. Then

$$\mathbb{P}\{h(\boldsymbol{G}) \geq \mathbb{E}(h(\boldsymbol{G})) + Lt\} \leq e^{-t^2/2}.$$

Now we are ready to present the main proof of Theorem 1.

$$\begin{aligned}
\|\boldsymbol{A} - \boldsymbol{Q}\boldsymbol{Q}^*\boldsymbol{A}\|_F^2 &\overset{(a)}{\leq} \|\boldsymbol{\Sigma}_2\|_F^2 + \|\boldsymbol{\Sigma}_2\boldsymbol{\Omega}_2\boldsymbol{\Omega}_1^\dagger\|_F^2 \\
&= \|\boldsymbol{\Sigma}_2\|_F^2 + \|\boldsymbol{\Sigma}_2(\boldsymbol{V}_2^*)^{(:,\Theta)}\boldsymbol{\Omega}^*\boldsymbol{\Omega}_1^\dagger\|_F^2 \\
&= \|\boldsymbol{\Sigma}_2\|_F^2 + \|\boldsymbol{\Sigma}_2(\boldsymbol{V}_2^*)^{(:,\Theta)}\boldsymbol{\Omega}^*((\boldsymbol{V}_1^*)^{(:,\Theta)}\boldsymbol{\Omega}^*)^\dagger\|_F^2 \\
&\overset{(b)}{=} \|\boldsymbol{\Sigma}_2\|_F^2 + \|\boldsymbol{\Sigma}_2(\boldsymbol{V}_2^*)^{(:,\Theta)}\boldsymbol{\Omega}^*(\boldsymbol{W}_2\boldsymbol{\Lambda}\boldsymbol{W}_1^*\boldsymbol{\Omega}^*)^\dagger\|_F^2
\end{aligned}$$

13

$$\overset{(c)}{=} \|\boldsymbol{\Sigma}_2\|_F^2 + \|\boldsymbol{\Sigma}_2(\boldsymbol{V}_2^*)^{(:,\Theta)}\boldsymbol{\Omega}^*(\boldsymbol{W}_1^*\boldsymbol{\Omega}^*)^\dagger\boldsymbol{\Lambda}^\dagger\boldsymbol{W}_2^\dagger\|_F^2$$

$$\leq \|\boldsymbol{\Sigma}_2\|_F^2 + \|(\boldsymbol{W}_1^*\boldsymbol{\Omega}^*)^\dagger\boldsymbol{\Lambda}^\dagger\boldsymbol{W}_2^\dagger\|_2^2 \cdot \|\boldsymbol{\Sigma}_2(\boldsymbol{V}_2^*)^{(:,\Theta)}\boldsymbol{\Omega}^*\|_F^2$$

$$\leq \|\boldsymbol{\Sigma}_2\|_F^2 + \|\boldsymbol{\Lambda}^\dagger\|_2^2 \cdot \|(\boldsymbol{W}_1^*\boldsymbol{\Omega}^*)^\dagger\|_2^2 \cdot \|\boldsymbol{\Sigma}_2(\boldsymbol{V}_2^*)^{(:,\Theta)}\boldsymbol{\Omega}^*\|_F^2$$

$$\overset{(d)}{\leq} \|\boldsymbol{\Sigma}_2\|_F^2 + \frac{6N}{n} \cdot \|(\boldsymbol{W}_1^*\boldsymbol{\Omega}^*)^\dagger\|_2^2 \cdot \|\boldsymbol{\Sigma}_2(\boldsymbol{V}_2^*)^{(:,\Theta)}\boldsymbol{\Omega}^*\|_F^2$$

$$\overset{(e)}{\leq} \|\boldsymbol{\Sigma}_2\|_F^2 + \frac{6N}{n} \cdot \frac{e^2 k^{1+6/(k-r+1)}}{(k-r+1)^2} \cdot \underbrace{\|\boldsymbol{\Sigma}_2(\boldsymbol{V}_2^*)^{(:,\Theta)}\boldsymbol{\Omega}^*\|_F^2}_{T_1},$$

where (a) holds with probability at least $1 - \frac{2}{r^3}$, by applying Lemma 1, Lemma 2, and Lemma 3; in (b), we assume $\boldsymbol{V}_1^{(\Theta,:)} = \boldsymbol{W}_1\boldsymbol{\Lambda}\boldsymbol{W}_2^*$ is the SVD (of rank r); (c) is due to the property of pseudo-inverse; (d) is due to the lower bound of the singular value in Lemma 1; (e) holds with probability at least $1 - \frac{1}{k^3}$, by applying Lemma 4 to $\boldsymbol{\Omega}\boldsymbol{W}_1$.

Bound for T_1. By Lemma 5,

$$\mathbb{E}(\|\boldsymbol{\Sigma}_2(\boldsymbol{V}_2^*)^{(:,\Theta)}\boldsymbol{\Omega}^*\|_F^2) = \|\boldsymbol{\Sigma}_2(\boldsymbol{V}_2^*)^{(:,\Theta)}\|_F^2 \cdot \|\boldsymbol{I}_k\|_F^2 \leq k\|\boldsymbol{\Sigma}_2\|_F^2,$$

where $\boldsymbol{I}_k$ is the identity matrix of size k, and the last inequality is due to $\|(\boldsymbol{V}_2^*)^{(:,\Theta)}\|_2 = \|\boldsymbol{V}_2^{(\Theta,:)}\|_2 \leq 1$. Consider the function $h(\boldsymbol{X}) = \|\boldsymbol{\Sigma}_2(\boldsymbol{V}_2^*)^{(:,\Theta)}\boldsymbol{X}\|_F$,

$$|h(\boldsymbol{X}) - h(\boldsymbol{Y})| = |\|\boldsymbol{\Sigma}_2(\boldsymbol{V}_2^*)^{(:,\Theta)}\boldsymbol{X}\|_F - \|\boldsymbol{\Sigma}_2(\boldsymbol{V}_2^*)^{(:,\Theta)}\boldsymbol{Y}\|_F|$$

$$\leq \|\boldsymbol{\Sigma}_2(\boldsymbol{V}_2^*)^{(:,\Theta)}(\boldsymbol{X} - \boldsymbol{Y})\|_F$$

$$\leq \|\boldsymbol{\Sigma}_2(\boldsymbol{V}_2^*)^{(:,\Theta)}\|_2 \cdot \|\boldsymbol{X} - \boldsymbol{Y}\|_F \leq \|\boldsymbol{\Sigma}_2\|_2 \cdot \|\boldsymbol{X} - \boldsymbol{Y}\|_F.$$

Thus the Lipschitz constant is $\|\boldsymbol{\Sigma}_2\|_2$. Now by Lemma 6, with probability at least $1 - e^{-t^2/2}$,

$$\|\boldsymbol{\Sigma}_2(\boldsymbol{V}_2^*)^{(:,\Theta)}\boldsymbol{\Omega}^*\|_F \leq \sqrt{k}\|\boldsymbol{\Sigma}_2\|_F + \|\boldsymbol{\Sigma}_2\|_2 \cdot t.$$

A particular choice of $t = \sqrt{6\log k}$ gives

$$\|\boldsymbol{\Sigma}_2(\boldsymbol{V}_2^*)^{(:,\Theta)}\boldsymbol{\Omega}^*\|_F \leq \sqrt{k}\|\boldsymbol{\Sigma}_2\|_F + \sqrt{6\log k}\|\boldsymbol{\Sigma}_2\|_2$$

with probability at least $1 - \frac{1}{k^3}$.

Based on the derived bound for T_1,

$$\|\boldsymbol{A} - \boldsymbol{Q}\boldsymbol{Q}^*\boldsymbol{A}\|_F \leq \sqrt{\|\boldsymbol{\Sigma}_2\|_F^2 + \frac{6N}{n} \cdot \frac{e^2 k^{1+6/(k-r+1)}}{(k-r+1)^2} \cdot \left(\sqrt{k}\|\boldsymbol{\Sigma}_2\|_F + \sqrt{6\log k}\|\boldsymbol{\Sigma}_2\|_2\right)^2}$$

$$\leq \|\boldsymbol{\Sigma}_2\|_F + \sqrt{\frac{6N}{n}} \cdot \frac{e\sqrt{k}}{k-r+1} \cdot k^{\frac{3}{k-r+1}} \cdot \left(\sqrt{k}\|\boldsymbol{\Sigma}_2\|_F + \sqrt{6\log k}\|\boldsymbol{\Sigma}_2\|_2\right)$$

$$= (C_1(p,k,r) + 1) \cdot \|\boldsymbol{\Sigma}_2\|_F + C_2(p,k,r) \cdot \|\boldsymbol{\Sigma}_2\|_2,$$

where the second inequality is due to $\sqrt{a^2 + b^2} \leq a + b$ for $a, b \geq 0$, and in the last equality,

$$C_1(p,k,r) = \sqrt{\frac{6e^2}{p} \cdot \frac{k}{k-r+1} \cdot k^{\frac{3}{k-r+1}}},$$

$$C_2(p,k,r) = \sqrt{\frac{36e^2}{p} \cdot \frac{\sqrt{k\log k}}{k-r+1} \cdot k^{\frac{3}{k-r+1}}}.$$

14

B.1 Proof of Lemma 3

First, the left unitary factor U plays no essential role. To see this, define

$$\widetilde{A} = U^* A = \begin{bmatrix} \Sigma_1 V_1^* \\ \Sigma_2 V_2^* \end{bmatrix} \quad \text{and} \quad \widetilde{Y} = \widetilde{A}^{(:,\Theta)} \Omega^* = \begin{bmatrix} \Sigma_1 \Omega_1 \\ \Sigma_2 \Omega_2 \end{bmatrix}.$$

Denote P_Y as the projection to the column space of Y. We have

$$\begin{aligned}
\|(I - P_Y)A\|_F &= \|(I - QQ^*)A\|_F \\
&= \|U^*(I - QQ^*)U\widetilde{A}\|_F \\
&= \|(I - (U^*Q)(U^*Q)^*)\widetilde{A}\|_F = \|(I - P_{\widetilde{Y}})\widetilde{A}\|_F.
\end{aligned}$$

It suffices to prove that

$$\|(I - P_{\widetilde{Y}})\widetilde{A}\|_F^2 \leq \|\Sigma_2\|_F^2 + \|\Sigma_2 \Omega_2 \Omega_1^\dagger\|_F^2.$$

Second, we assume that Σ_2 is not zero matrix. Otherwise,

$$\text{range}(\widetilde{A}) = \text{range}\left(\begin{bmatrix} \Sigma_1 V_1^* \\ 0 \end{bmatrix}\right) = \text{range}\left(\begin{bmatrix} \Sigma_1 \Omega_1 \\ 0 \end{bmatrix}\right) = \text{range}(\widetilde{Y}),$$

where the second equality holds since both V_1^* and Ω_1 have full row rank. As the result,

$$\|(I - P_{\widetilde{Y}})\widetilde{A}\|_F = 0,$$

and the conclusion follows.

Next, we flatten out the top block of $\widetilde{Y}$ to obtain

$$Z = \widetilde{Y} \cdot \Omega_1^\dagger \Sigma_1^{-1} = \begin{bmatrix} I \\ F \end{bmatrix}, \quad \text{where} \quad F = \Sigma_2 \Omega_2 \Omega_1^\dagger \Sigma_1^{-1}.$$

Since $\text{range}(Z) \subset \text{range}(\widetilde{Y})$,

$$\|(I - P_{\widetilde{Y}})\widetilde{A}\|_F \leq \|(I - P_Z)\widetilde{A}\|_F$$

by applying [8, Proposition 8.5]. Taking squares,

$$\|(I - P_{\widetilde{Y}})\widetilde{A}\|_F^2 \leq \|(I - P_Z)\widetilde{A}\|_F^2 = \text{Tr}(\widetilde{A}^*(I - P_Z)\widetilde{A}) = \text{Tr}(\Sigma(I - P_Z)\Sigma).$$

Note that Z has full column rank,

$$P_Z = Z(Z^*Z)^{-1}Z^* = \begin{bmatrix} I \\ F \end{bmatrix}(I + F^*F)^{-1}\begin{bmatrix} I \\ F \end{bmatrix}^*,$$

and $I - P_Z$ is equal to

$$\begin{bmatrix} I - (I + F^*F)^{-1} & -(I + F^*F)^{-1}F^* \\ -F(I + F^*F)^{-1} & I - F(I + F^*F)^{-1}F^* \end{bmatrix}.$$

The top left block satisfies

$$I - (I + F^*F)^{-1} \preceq F^*F$$

by applying [8, Proposition 8.2], and the bottom right block satisfies

$$I - F(I + F^*F)^{-1}F^* \preceq I$$

since $F(I + F^*F)^{-1}F^* \succeq 0$. Denote $B = -(I + F^*F)^{-1}F^*$,

$$I - P_Z \preceq \begin{bmatrix} F^*F & B \\ B^* & I \end{bmatrix},$$

and consequently,

$$\Sigma(I - P_Z)\Sigma \preceq \begin{bmatrix} \Sigma_1 F^*F\Sigma_1 & \Sigma_1 B\Sigma_2 \\ \Sigma_2 B^*\Sigma_1 & \Sigma_2^2 \end{bmatrix}.$$

The last step is to note that

$$\begin{aligned}
\mathrm{Tr}(\Sigma(I - P_Z)\Sigma) \leq & \mathrm{Tr}\left(\begin{bmatrix} \Sigma_1 F^*F\Sigma_1 & \Sigma_1 B\Sigma_2 \\ \Sigma_2 B^*\Sigma_1 & \Sigma_2^2 \end{bmatrix} \right) \\
= & \mathrm{Tr}(\Sigma_1 F^*F\Sigma_1) + \mathrm{Tr}(\Sigma_2^2) \\
= & \|F\Sigma_1\|_F^2 + \|\Sigma_2\|_F^2 \\
= & \|\Sigma_2\Omega_2\Omega_1^\dagger\|_F^2 + \|\Sigma_2\|_F^2.
\end{aligned}$$

C   Proof of Theorem 2

The final approximation $[[\hat{A}]]_r$ is the best rank r approximation of $\hat{A}$. Note that

$$\begin{aligned}
\|A - [[\hat{A}]]_r\|_F \leq & \|A - \hat{A}\|_F + \|\hat{A} - [[\hat{A}]]_r\|_F \\
\leq & \|A - \hat{A}\|_F + \|\hat{A} - [[A]]_r\|_F \\
\leq & 2\|A - \hat{A}\|_F + \|A - [[A]]_r\|_F \\
= & 2\|A - \hat{A}\|_F + \|\Sigma_2\|_F,
\end{aligned}$$

where the second inequality holds since $[[\hat{A}]]_r$ is the best rank r approximation to $\hat{A}$. We could bound $\|A - [[\hat{A}]]_r\|_F$ by bounding the initial approximation error $\|A - \hat{A}\|_F$.

$$\begin{aligned}
\|A - \hat{A}\|_F^2 = & \|A - QCP^*\|_F^2 \\
= & \|A - QQ^*APP^* + Q(Q^*AP - C)P^*\|_F^2 \\
= & \|A - QQ^*APP^*\|_F^2 + \|Q(C - Q^*AP)P^*\|_F^2 \\
= & \underbrace{\|A - QQ^*APP^*\|_F^2}_{T_2} + \underbrace{\|C - Q^*AP\|_F^2}_{T_3},
\end{aligned}$$

where the third equality is due to

$$\langle A - QQ^*APP^*, Q(C - Q^*AP)P^* \rangle = \langle Q^*(A - QQ^*APP^*)P, C - Q^*AP \rangle = 0.$$

Bound for T_2. Note that

$$T_2 = \|A(I - PP^*) + (I - QQ^*)APP^*\|_F^2$$

16

$$\begin{aligned}
&= \|\boldsymbol{A}(\boldsymbol{I} - \boldsymbol{P}\boldsymbol{P}^*)\|_F^2 + \|(\boldsymbol{I} - \boldsymbol{Q}\boldsymbol{Q}^*)\boldsymbol{A}\boldsymbol{P}\boldsymbol{P}^*\|_F^2 \\
&= \|\boldsymbol{A}(\boldsymbol{I} - \boldsymbol{P}\boldsymbol{P}^*)\|_F^2 + \|(\boldsymbol{I} - \boldsymbol{Q}\boldsymbol{Q}^*)\boldsymbol{A}\boldsymbol{P}\|_F^2 \\
&= \|(\boldsymbol{U}_2\boldsymbol{\Sigma}_2\boldsymbol{V}_2^*)(\boldsymbol{I} - \boldsymbol{P}\boldsymbol{P}^*)\|_F^2 + \|(\boldsymbol{U}_1\boldsymbol{\Sigma}_1\boldsymbol{V}_1^*)(\boldsymbol{I} - \boldsymbol{P}\boldsymbol{P}^*)\|_F^2 + \|(\boldsymbol{I} - \boldsymbol{Q}\boldsymbol{Q}^*)\boldsymbol{A}\boldsymbol{P}\|_F^2 \\
&\leq \|\boldsymbol{\Sigma}_2\|_F^2 + \|(\boldsymbol{U}_1\boldsymbol{\Sigma}_1\boldsymbol{V}_1^*)(\boldsymbol{I} - \boldsymbol{P}\boldsymbol{P}^*)\|_F^2 + \|(\boldsymbol{I} - \boldsymbol{Q}\boldsymbol{Q}^*)\boldsymbol{A}\boldsymbol{P}\|_F^2,
\end{aligned}$$

where the second equality is due to

$$\langle \boldsymbol{A}(\boldsymbol{I} - \boldsymbol{P}\boldsymbol{P}^*), (\boldsymbol{I} - \boldsymbol{Q}\boldsymbol{Q}^*)\boldsymbol{A}\boldsymbol{P}\boldsymbol{P}^* \rangle = 0,$$

and the fourth equality is due to

$$\langle (\boldsymbol{U}_2\boldsymbol{\Sigma}_2\boldsymbol{V}_2^*)(\boldsymbol{I} - \boldsymbol{P}\boldsymbol{P}^*), (\boldsymbol{U}_1\boldsymbol{\Sigma}_1\boldsymbol{V}_1^*)(\boldsymbol{I} - \boldsymbol{P}\boldsymbol{P}^*) \rangle = 0.$$

Denote $\boldsymbol{\Gamma}_1 = \boldsymbol{\Gamma}\boldsymbol{U}_1^{(\Delta,:)}$, and $\boldsymbol{\Gamma}_2 = \boldsymbol{\Gamma}\boldsymbol{U}_2^{(\Delta,:)}$. Following a similar argument as the proof of Lemma 3,

$$\|(\boldsymbol{U}_1\boldsymbol{\Sigma}_1\boldsymbol{V}_1^*)(\boldsymbol{I} - \boldsymbol{P}\boldsymbol{P}^*)\|_F^2 \leq \|\boldsymbol{\Gamma}_1^\dagger\boldsymbol{\Gamma}_2\boldsymbol{\Sigma}_2\|_F^2.$$

Therefore, we arrive at

$$\begin{aligned}
T_2 &\leq \|\boldsymbol{\Sigma}_2\|_F^2 + \|\boldsymbol{\Gamma}_1^\dagger\boldsymbol{\Gamma}_2\boldsymbol{\Sigma}_2\|_F^2 + \|(\boldsymbol{I} - \boldsymbol{Q}\boldsymbol{Q}^*)\boldsymbol{A}\boldsymbol{P}\|_F^2 \\
&\leq \|\boldsymbol{\Sigma}_2\|_F^2 + \|\boldsymbol{\Gamma}_1^\dagger\boldsymbol{\Gamma}_2\boldsymbol{\Sigma}_2\|_F^2 + \|(\boldsymbol{I} - \boldsymbol{Q}\boldsymbol{Q}^*)\boldsymbol{A}\|_F^2 \\
&\leq \|\boldsymbol{\Sigma}_2\|_F^2 + \|\boldsymbol{\Gamma}_1^\dagger\boldsymbol{\Gamma}_2\boldsymbol{\Sigma}_2\|_F^2 + \|\boldsymbol{\Sigma}_2\|_F^2 + \|\boldsymbol{\Sigma}_2\boldsymbol{\Omega}_2\boldsymbol{\Omega}_1^\dagger\|_F^2 \\
&= 2\|\boldsymbol{\Sigma}_2\|_F^2 + \|\boldsymbol{\Gamma}_1^\dagger\boldsymbol{\Gamma}_2\boldsymbol{\Sigma}_2\|_F^2 + \|\boldsymbol{\Sigma}_2\boldsymbol{\Omega}_2\boldsymbol{\Omega}_1^\dagger\|_F^2.
\end{aligned}$$

Bound for T_3. We decompose $\boldsymbol{C} - \boldsymbol{Q}^*\boldsymbol{A}\boldsymbol{P}$ into several parts, and bound them separately. Denote the complement of $\boldsymbol{Q}$ and $\boldsymbol{P}$ to be $\boldsymbol{Q}_\perp$ and $\boldsymbol{P}_\perp$, respectively. Define

$$\boldsymbol{\Phi}_1 = \boldsymbol{\Phi}\boldsymbol{Q}^{(\Delta',:)} \quad \text{and} \quad \boldsymbol{\Phi}_2 = \boldsymbol{\Phi}\boldsymbol{Q}_\perp^{(\Delta',:)},$$

$$\boldsymbol{\Psi}_1 = \boldsymbol{\Psi}\boldsymbol{P}^{(\Theta',:)} \quad \text{and} \quad \boldsymbol{\Psi}_2 = \boldsymbol{\Psi}\boldsymbol{P}_\perp^{(\Theta',:)}.$$

Lemma 7. *Assume that $\boldsymbol{\Phi}_1$ and $\boldsymbol{\Psi}_1$ are of full column rank. Then*

$$\boldsymbol{C} - \boldsymbol{Q}^*\boldsymbol{A}\boldsymbol{P} = \boldsymbol{\Phi}_1^\dagger\boldsymbol{\Phi}_2(\boldsymbol{Q}_\perp^*\boldsymbol{A}\boldsymbol{P}) + (\boldsymbol{Q}^*\boldsymbol{A}\boldsymbol{P}_\perp)\boldsymbol{\Psi}_2^*(\boldsymbol{\Psi}_1^\dagger)^* + \boldsymbol{\Phi}_1^\dagger\boldsymbol{\Phi}_2(\boldsymbol{Q}_\perp^*\boldsymbol{A}\boldsymbol{P}_\perp)\boldsymbol{\Psi}_2^*(\boldsymbol{\Psi}_1^\dagger)^*.$$

The proof of Lemma 7 is the same as [14, Lemma A.3]. For completeness, we include its proof in Section C.1.

Remark. *To ensure that $\boldsymbol{\Phi}_1$ and $\boldsymbol{\Psi}_1$ are of full column rank, one way is to argue that $\boldsymbol{Q}$ and $\boldsymbol{P}$ are also incoherent, i.e.,*

$$\max_i \left\{ \|\boldsymbol{Q}^{(i,:)}\|_2 \right\} \leq \sqrt{\frac{\mu' k}{M}} \quad \text{and} \quad \max_j \left\{ \|\boldsymbol{P}^{(j,:)}\|_2 \right\} \leq \sqrt{\frac{\nu' k}{N}} \tag{2}$$

for some $\mu' \ll M$, $\nu' \ll N$, and apply Lemma 1. As shown in the following table, we empirically observe that (2) holds, and the incoherence parameters $\mu' = O(\mu)$, $\nu' = O(\nu)$. Table 6 also confirms that (μ, ν) and (μ', ν') are indeed small, compared to matrix size (M, N), for all the datasets.

	Yale Face	Cardiac MRI	BR1003	Video
μ	4.1137	127.5935	5.4270	20.3505
μ'	5.9454	159.8982	5.2750	22.8109
ν	2.7068	2.1507	32.8387	14.0194
ν'	4.1355	2.2260	57.4357	6.7429

Table 6: Comparison of (μ, ν) and (μ', ν') on different datasets. The parameters (r, k, s, p) for each dataset are chosen as the same values as used to show all the visual comparisons.

However, we find that our theoretical bounds of (μ', ν') in (2) are currently difficult to prove. One way to get around this is to slightly modify the algorithm: after building the left and right sketches, we calculate the QR factorizations, and sample m' row indices and n' column indices based on the actual incoherence parameters, estimated from the row norms, of $\boldsymbol{Q}$ and $\boldsymbol{P}$, respectively. Then we sample $m' \approx O(\mu' k \log k)$ row indices, and $n' \approx O(\nu' k \log k)$ column indices to get the data in the intersection.

$$T_3 = \|\boldsymbol{\Phi}_1^{\dagger}\boldsymbol{\Phi}_2(\boldsymbol{Q}_{\perp}^*\boldsymbol{A}\boldsymbol{P}) + (\boldsymbol{Q}^*\boldsymbol{A}\boldsymbol{P}_{\perp})\boldsymbol{\Psi}_2^*(\boldsymbol{\Psi}_1^{\dagger})^* + \boldsymbol{\Phi}_1^{\dagger}\boldsymbol{\Phi}_2(\boldsymbol{Q}_{\perp}^*\boldsymbol{A}\boldsymbol{P}_{\perp})\boldsymbol{\Psi}_2^*(\boldsymbol{\Psi}_1^{\dagger})^*\|_F^2$$
$$\leq 3 \cdot (\underbrace{\|\boldsymbol{\Phi}_1^{\dagger}\boldsymbol{\Phi}_2(\boldsymbol{Q}_{\perp}^*\boldsymbol{A}\boldsymbol{P})\|_F^2}_{T_{31}} + \underbrace{\|(\boldsymbol{Q}^*\boldsymbol{A}\boldsymbol{P}_{\perp})\boldsymbol{\Psi}_2^*(\boldsymbol{\Psi}_1^{\dagger})^*\|_F^2}_{T_{32}} + \underbrace{\|\boldsymbol{\Phi}_1^{\dagger}\boldsymbol{\Phi}_2(\boldsymbol{Q}_{\perp}^*\boldsymbol{A}\boldsymbol{P}_{\perp})\boldsymbol{\Psi}_2^*(\boldsymbol{\Psi}_1^{\dagger})^*\|_F^2}_{T_{33}}).$$

We bound the three terms separately. The bounds all follow from a similar argument as deriving the bound for $\|\boldsymbol{\Sigma}_2\boldsymbol{\Omega}_2\boldsymbol{\Omega}_1^{\dagger}\|_F^2$ in the proof of Theorem 1. Suppose $s \geq k + 4$.

$$T_{31} \leq \frac{6e^2}{q} \cdot \frac{s^{1+6/(s-k+1)}}{(s-k+1)^2} \cdot \left(\sqrt{s}\|\boldsymbol{Q}_{\perp}^*\boldsymbol{A}\boldsymbol{P}\|_F + \sqrt{6\log s}\|\boldsymbol{Q}_{\perp}^*\boldsymbol{A}\boldsymbol{P}\|_2\right)^2$$
$$\leq \frac{6e^2}{q} \cdot \frac{s^{1+6/(s-k+1)}}{(s-k+1)^2} \cdot \left(\sqrt{s} + \sqrt{6\log s}\right)^2 \cdot \|\boldsymbol{Q}_{\perp}^*\boldsymbol{A}\boldsymbol{P}\|_F^2$$
$$= C(q, s, k) \cdot \|\boldsymbol{Q}_{\perp}^*\boldsymbol{A}\boldsymbol{P}\|_F^2$$

with probability at least $1 - \frac{2}{s^3}$, where

$$C(q, s, k) = \frac{6e^2}{q} \cdot \frac{s^{1+6/(s-k+1)}}{(s-k+1)^2} \cdot \left(\sqrt{s} + \sqrt{6\log s}\right)^2.$$

Similarly, with probability at least $1 - \frac{2}{s^3}$,

$$T_{32} \leq C(q, s, k) \cdot \|\boldsymbol{Q}^*\boldsymbol{A}\boldsymbol{P}_{\perp}\|_F^2.$$

Apply the argument twice,

$$T_{33} \leq C(q, s, k) \cdot \|(\boldsymbol{Q}_{\perp}^*\boldsymbol{A}\boldsymbol{P}_{\perp})\boldsymbol{\Psi}_2^*(\boldsymbol{\Psi}_1^{\dagger})^*\|_F^2 \leq (C(q, s, k))^2 \cdot \|\boldsymbol{Q}_{\perp}^*\boldsymbol{A}\boldsymbol{P}_{\perp}\|_F^2$$

with probability at least $1 - \frac{2}{s^2}$. Combining the three estimates,

$$\frac{T_3}{3} \leq C(q, s, k) \cdot \left(\|\boldsymbol{Q}_{\perp}^*\boldsymbol{A}\boldsymbol{P}\|_F^2 + \|\boldsymbol{Q}^*\boldsymbol{A}\boldsymbol{P}_{\perp}\|_F^2 + C(q, s, k) \cdot \|\boldsymbol{Q}_{\perp}^*\boldsymbol{A}\boldsymbol{P}_{\perp}\|_F^2\right)$$

$$
\begin{aligned}
=&C(q,s,k)\cdot\left(\|\boldsymbol{Q}_\perp^*\boldsymbol{AP}\|_F^2+\|\boldsymbol{Q}^*\boldsymbol{AP}_\perp\|_F^2+\|\boldsymbol{Q}_\perp^*\boldsymbol{AP}_\perp\|_F^2+(C(q,s,k)-1)\cdot\|\boldsymbol{Q}_\perp^*\boldsymbol{AP}_\perp\|_F^2\right)\\
=&C(q,s,k)\cdot\left(\|\boldsymbol{A}-\boldsymbol{QQ}^*\boldsymbol{APP}^*\|_F^2+(C(q,s,k)-1)\cdot\|\boldsymbol{Q}_\perp^*\boldsymbol{AP}_\perp\|_F^2\right)\\
=&C(q,s,k)\cdot\|\boldsymbol{A}-\boldsymbol{QQ}^*\boldsymbol{APP}^*\|_F^2+C(q,s,k)(C(q,s,k)-1)\cdot\|\boldsymbol{Q}_\perp\boldsymbol{Q}_\perp^*\boldsymbol{AP}_\perp\|_F^2\\
\leq&C(q,s,k)\cdot\|\boldsymbol{A}-\boldsymbol{QQ}^*\boldsymbol{APP}^*\|_F^2+C(q,s,k)(C(q,s,k)-1)\cdot\|(\boldsymbol{I}-\boldsymbol{QQ}^*)\boldsymbol{A}\|_F^2.
\end{aligned}
$$

Thus for the square of the initial approximation error,

$$
\begin{aligned}
\|\boldsymbol{A}-\hat{\boldsymbol{A}}\|_F^2\leq&(3C(q,s,k)+1)\cdot\|\boldsymbol{A}-\boldsymbol{QQ}^*\boldsymbol{APP}^*\|_F^2\\
&+3C(q,s,k)(C(q,s,k)-1)\cdot\|(\boldsymbol{I}-\boldsymbol{QQ}^*)\boldsymbol{AP}\|_F^2\\
\leq&(3C(q,s,k)+1)\cdot(2\|\boldsymbol{\Sigma}_2\|_F^2+\|\boldsymbol{\Gamma}_1^\dagger\boldsymbol{\Gamma}_2\boldsymbol{\Sigma}_2\|_F^2+\|\boldsymbol{\Sigma}_2\boldsymbol{\Omega}_2\boldsymbol{\Omega}_1^\dagger\|_F^2)\\
&+3C(q,s,k)(C(q,s,k)-1)\cdot(\|\boldsymbol{\Sigma}_2\|_F^2+\|\boldsymbol{\Sigma}_2\boldsymbol{\Omega}_2\boldsymbol{\Omega}_1^\dagger\|_F^2).
\end{aligned}
$$

Taking the square root,

$$
\begin{aligned}
\|\boldsymbol{A}-\hat{\boldsymbol{A}}\|_F\leq&\sqrt{3(C(q,s,k))^2+3C(q,s,k)+2}\cdot(C_1(p,k,r)\|\boldsymbol{\Sigma}_2\|_F+C_2(p,k,r)\|\boldsymbol{\Sigma}_2\|_2)\\
\leq&(\sqrt{3}C(q,s,k)+\sqrt{2})\cdot(C_1(p,k,r)\|\boldsymbol{\Sigma}_2\|_F+C_2(p,k,r)\|\boldsymbol{\Sigma}_2\|_2)\\
=&C_3(p,q,s,k,r)\cdot\|\boldsymbol{\Sigma}_2\|_F+C_4(p,q,s,k,r)\cdot\|\boldsymbol{\Sigma}_2\|_2,
\end{aligned}
$$

where

$$
\begin{aligned}
C_3(p,q,s,k,r)=&C_1(p,k,r)\cdot(\sqrt{3}C(q,s,k)+\sqrt{2}),\\
C_4(p,q,s,k,r)=&C_2(p,k,r)\cdot(\sqrt{3}C(q,s,k)+\sqrt{2}).
\end{aligned}
$$

C.1 Proof of Lemma 7

Define $\boldsymbol{S}_{\Delta'}\in\mathbb{R}^{m'\times M}$ such that when left multiplied to a matrix, the result is equal to the rows with indices Δ' of that matrix. Define $\boldsymbol{S}_{\Theta'}$ similarly. The core sketch can be written as

$$
\begin{aligned}
\boldsymbol{Z}=&\boldsymbol{\Phi}\boldsymbol{A}^{(\Delta',\Theta')}\boldsymbol{\Psi}^*=\boldsymbol{\Phi}\boldsymbol{S}_{\Delta'}\boldsymbol{A}\boldsymbol{S}_{\Theta'}^*\boldsymbol{\Psi}^*\\
=&\boldsymbol{\Phi}\boldsymbol{S}_{\Delta'}(\boldsymbol{A}-\boldsymbol{QQ}^*\boldsymbol{APP}^*)\boldsymbol{S}_{\Theta'}^*\boldsymbol{\Psi}^*+(\boldsymbol{\Phi}\boldsymbol{S}_{\Delta'}\boldsymbol{Q})\boldsymbol{Q}^*\boldsymbol{AP}(\boldsymbol{P}^*\boldsymbol{S}_{\Theta'}^*\boldsymbol{\Psi}^*)\\
=&\boldsymbol{\Phi}\boldsymbol{S}_{\Delta'}(\boldsymbol{A}-\boldsymbol{QQ}^*\boldsymbol{APP}^*)\boldsymbol{S}_{\Theta'}^*\boldsymbol{\Psi}^*+(\boldsymbol{\Phi}\boldsymbol{Q}^{(\Delta',:)})\boldsymbol{Q}^*\boldsymbol{AP}(\boldsymbol{\Psi}\boldsymbol{P}^{(\Theta',:)})^*.
\end{aligned}
$$

Left multiply by $\boldsymbol{\Phi}_1^\dagger$ and right-multiply by $(\boldsymbol{\Psi}_1^\dagger)^*$,

$$
\boldsymbol{C}=\boldsymbol{\Phi}_1^\dagger\boldsymbol{\Phi}\boldsymbol{S}_{\Delta'}(\boldsymbol{A}-\boldsymbol{QQ}^*\boldsymbol{APP}^*)\boldsymbol{S}_{\Theta'}^*\boldsymbol{\Psi}^*(\boldsymbol{\Psi}_1^\dagger)^*+\boldsymbol{Q}^*\boldsymbol{AP}.
$$

Notice that

$$
\begin{aligned}
\boldsymbol{\Phi}_1^\dagger\boldsymbol{\Phi}\boldsymbol{S}_{\Delta'}&=\boldsymbol{\Phi}_1^\dagger\boldsymbol{\Phi}\boldsymbol{S}_{\Delta'}\boldsymbol{QQ}^*+\boldsymbol{\Phi}_1^\dagger\boldsymbol{\Phi}\boldsymbol{S}_{\Delta'}\boldsymbol{Q}_\perp\boldsymbol{Q}_\perp^*=\boldsymbol{Q}^*+\boldsymbol{\Phi}_1^\dagger\boldsymbol{\Phi}_2\boldsymbol{Q}_\perp^*,\\
\boldsymbol{S}_{\Theta'}^*\boldsymbol{\Psi}^*(\boldsymbol{\Psi}_1^\dagger)^*&=\boldsymbol{PP}^*\boldsymbol{S}_{\Theta'}^*\boldsymbol{\Psi}^*(\boldsymbol{\Psi}_1^\dagger)^*+\boldsymbol{P}_\perp\boldsymbol{P}_\perp^*\boldsymbol{S}_{\Theta'}^*\boldsymbol{\Psi}^*(\boldsymbol{\Psi}_1^\dagger)^*=\boldsymbol{P}+\boldsymbol{P}_\perp\boldsymbol{\Psi}_2^*(\boldsymbol{\Psi}_1^\dagger)^*.
\end{aligned}
$$

Combining all the pieces,

$$
\begin{aligned}
\boldsymbol{C}-\boldsymbol{Q}^*\boldsymbol{AP}=&\left(\boldsymbol{Q}^*+\boldsymbol{\Phi}_1^\dagger\boldsymbol{\Phi}_2\boldsymbol{Q}_\perp^*\right)(\boldsymbol{A}-\boldsymbol{QQ}^*\boldsymbol{APP}^*)\left(\boldsymbol{P}+\boldsymbol{P}_\perp\boldsymbol{\Psi}_2^*(\boldsymbol{\Psi}_1^\dagger)^*\right)\\
=&\boldsymbol{\Phi}_1^\dagger\boldsymbol{\Phi}_2(\boldsymbol{Q}_\perp^*\boldsymbol{AP})+(\boldsymbol{Q}^*\boldsymbol{AP}_\perp)\boldsymbol{\Psi}_2^*(\boldsymbol{\Psi}_1^\dagger)^*+\boldsymbol{\Phi}_1^\dagger\boldsymbol{\Phi}_2(\boldsymbol{Q}_\perp^*\boldsymbol{AP}_\perp)\boldsymbol{\Psi}_2^*(\boldsymbol{\Psi}_1^\dagger)^*.
\end{aligned}
$$

D More Numerics

We use a Navier Stokes simulated flow system which generates vorticity patterns for an incompressible fluid under certain initial and boundary conditions. For each point of the 100×50 grids, fluid velocity values in both x and y directions for 200 time instances. As an example we demonstrate our results on the y component of the fluid velocity, captured in the data matrix $A \in \mathbb{R}^{5000 \times 200}$. Based on the scree plot, we choose $r = 7$. The optimal err is 0.0016.
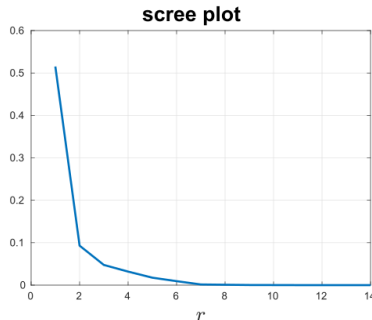
Figure 9: Scree plot for Navier Stokes dataset.

	SketchySVD	SketchyCoreSVD
p	-	0.3
err	0.0016	0.0016
time (sec)	0.0097	0.0062

Table 7: Performance comparisons for Navier Stokes dataset.

We choose $k = 4r + 1 = 29$ and $s = 2k + 1 = 59$ for both methods. In Table 7, we see that the error of SketchySVD is the same as the optimal error. SketchyCoreSVD can thus achieve the same error bound in less time. In the visual comparison Figure 10, we show that the singular vector(s) can be estimated accurately, and with sampling ratio $p = 30\%$ for SketchyCoreSVD. Table 8 further verifies that the PSNR ratios of the computed singular vectors are very high, and that SketchyCoreSVD achieves those ratios with only sampling ratio $p = 30\%$.

	1	2	3	4	5	6
SketchySVD	115.3884	116.2469	112.3364	96.8527	97.7459	88.7866
SketchyCoreSVD	107.3097	107.2117	98.2154	84.5132	83.6819	85.8143

Table 8: Comparison of PSNR ratios for the first six left singular vectors computed on the Navier Stokes dataset, where $p = 0.3$ for our SketchyCoreSVD method.
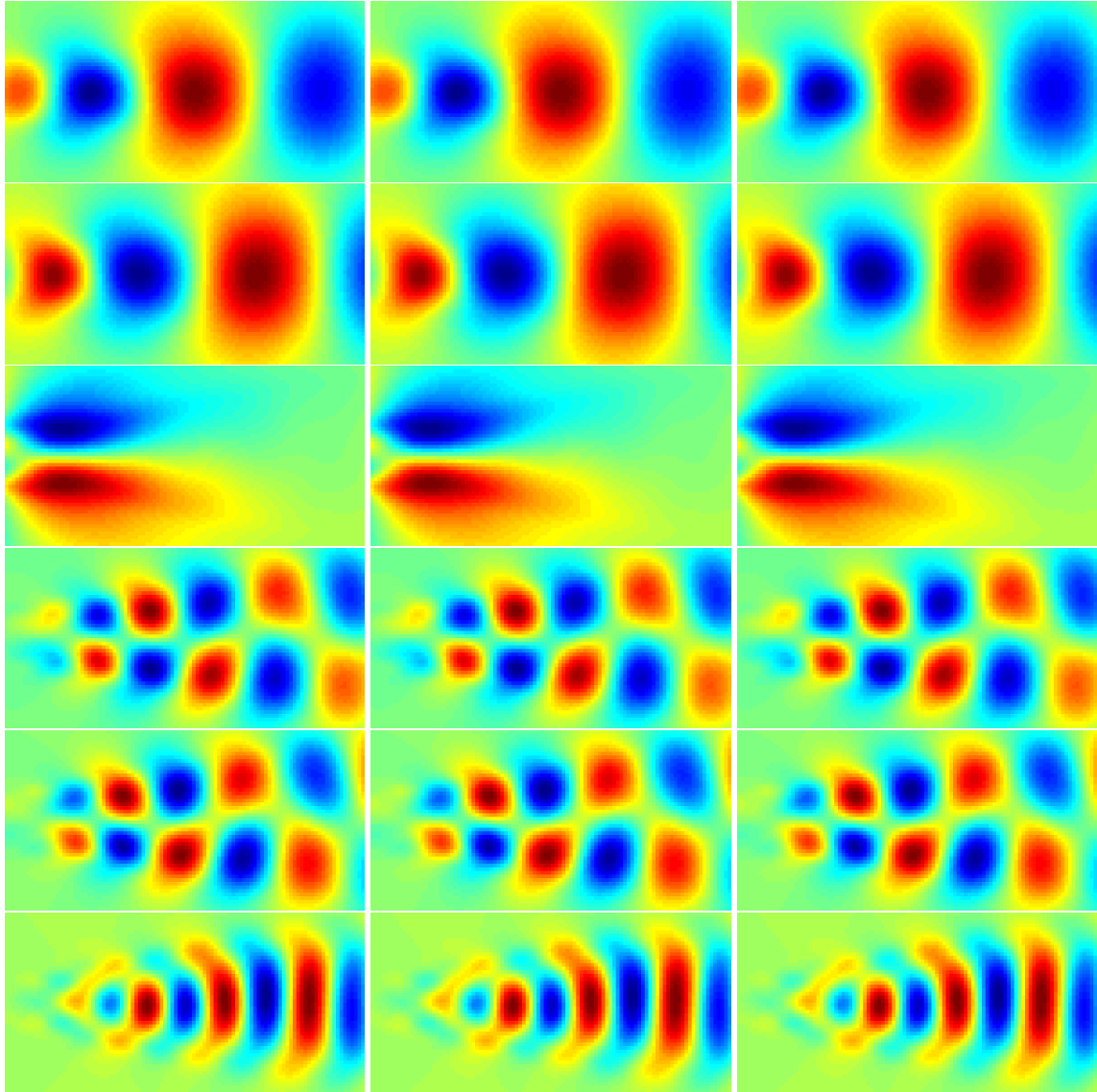
Figure 10: Visual comparison for the first six left singular vectors computed on the Navier Stokes dataset. Ground truth (left column), SketchySVD (middle column), SketchyCoreSVD (right column, $p = 0.3$). For each subfigure, $x \in [1, 8]$ (horizontal), and $y \in [-2, 2]$ (vertical).